Journal of Electronic Materials (2022) 51:3903–3918
https://doi.org/10.1007/s11664-022-09650-3

ORIGINAL RESEARCH ARTICLE

Electron Density and Optoelectronic Properties of Copper Antimony Sulphur Ternary Compounds for Photovoltaic Applications

Mohamed Khairy[1] · Pingping Jiang[2,3,4] · Pascal Boulet[2] · Marie-Christine Record[3]

Received: 7 December 2021 / Accepted: 11 April 2022 / Published online: 2 May 2022

Abstract

Design of efficient solar energy-conversion materials has attracted much interest in the last few decades. Among these materials, copper-based semiconducting chalcogenides have been employed as alternatives for copper indium gallium selenide thin-film solar cells due to their low toxicity and earth-abundant absorber components. In the present manuscript, structural, electronic, quantum theory of atoms in molecules (QTAIM) topological, and optical properties of ternary chalcogenide $CuSbS_2$, Cu_3SbS_3, and Cu_3SbS_4 have been investigated using the full potential linear augmented plane wave method. An indirect band gap is observed for $CuSbS_2$ with $E_g = 1.18$ eV and a direct band gap is found for Cu_3SbS_3, and Cu_3SbS_4 with $E_g = 1.28$ and 1.0 eV, respectively. The valence band maximum of $CuSbS_2$, Cu_3SbS_3, and Cu_3SbS_4 are mainly predominated by a strong Cu-3d and S-3p orbitals hybridization. The conduction band of $CuSbS_2$ and Cu_3SbS_3 are mainly characterized by Sb-5p orbital and S-3p orbital mixing. However, conduction band of Cu_3SbS_4 is dominated by the mixing of Sb-5s and S-3p orbitals. It is found that the Cu-S and Sb-S bonds lie in the transit closed-shell zone, between the typical ionic and covalent bonds, the Cu-S bonds being more ionic in nature and the Sb-S bonds being more covalent. The optical properties of $CuSbS_2$, Cu_3SbS_3, and Cu_3SbS_4 in terms of absorption coefficient, extinction coefficient, refractive index, and reflectivity have been investigated. It is found that Cu_3SbS_4 is probably less suitable for optical application than $CuSbS_2$ and Cu_3SbS_3 as the chemical bonds in Cu_3SbS_4 are seemingly less polarizable, as assumed from the QTAIM analysis, which seems to be correlated with a lower absorption coefficient.

Keywords Copper-based chalcogenides · DFT · optoelectronic properties · electron density topology · solar-energy conversion

Introduction

The search for and design of efficient solar energy-conversion materials have attracted much interest in the last few decades in order to overcome the global energy shortage and CO_2 emission in the inevitable future expansion.[1] In 2019, the producing capacity of solar photovoltaics (PV) reached about 633 GW, with a 24% growth year-on-year and might foresee reaching 4.7 TW by 2050 as proposed by the International Energy Agency (IEA). More than 90% of world production capacity is held by crystalline silicon modules, which are very effective. The cheaper thin-film compound semiconductors might be alternatives and strong competitors to silicon PV. Recently, transition metal chalcogenides have enabled a breakthrough in the development of thin-film photovoltaic solar cells because of their optoelectronic properties in terms of photo-stability and high surface area visible-light absorbance.[2] For example, copper indium gallium selenide (CIGS) and cadmium telluride (CdTe) solar cells revealed a spectroscopic limited maximum efficiency (SLME) of about 20.8% and 19.6%, respectively. Although these thin-film photovoltaic cells are commercially available, their elemental components are toxic and relatively rare, which limits their terawatt-scale productions.[3] Copper zinc tin sulfoselenide (CZTSSe) was explored as a promising alternative material because it might fulfill the

✉ Marie-Christine Record
m-c.record@univ-amu.fr

1 Chemistry Department, Faculty of Science, Sohag University, Sohag 82524, Egypt

2 CNRS, MADIREL, Aix-Marseille University, 13013 Marseille, France

3 CNRS, IM2NP, Aix-Marseille University, University of Toulon, 13013 Marseille, France

4 Present Address: INSA Rennes, CNRS, Institut FOTON - UMR 6082, Univ Rennes, 35000 Rennes, France

prerequisites for sufficient solar irradiation, but still, the efficiency of PV devices is relatively low, despite more than a decade of painstaking research.[4] The copper-based chalcogenide systems including $CuSbS_2$ (chalcostibite), Cu_3SbS_4 (famatinite), $Cu_{12}Sb_4S_{13}$ (tetrahedrite), and Cu_3SbS_3 (skinnerite) phases have been explored as they are interesting alternatives for CIGS thin-film solar cells due to their low-toxicity and earth-abundant absorber components.[3,5–13] The Cu-Sb-S system compounds are p-type semiconductors with an optical band gap (E_g) ranging between 0.5 eV and 2.0 eV and a large absorption coefficient over 10^4 cm^{-1} at visible wavelengths, which shows a comparable efficiency (i.e., 22.9%) to that of CIGS and CZTSSe.[14] Yet, due to a lack of knowledge in the fundamental physical properties comprehension these compounds have not reached the stage of integration into devices. Therefore, further developments in PV technology based on these compounds call for a deep understanding of the electronic and optical properties of these materials and of their structural properties relationships, which is the topic of the present work.

In this work, we have investigated the structural, electronic, and optical properties of ternary chalcogenide $CuSbS_2$, Cu_3SbS_3, and Cu_3SbS_4 using density functional theory (DFT) calculations with the full-potential linearized augmented plane-wave (FP-LAPW) method that was suggested to be one of the most efficient methods to solve many-electron problems in a solid crystal. $Cu_{12}Sb_4S_{13}$ has not been considered in the present work as it shows a semi-metallic behaviour.[3]

There are crucial needs for rationalizing the behaviour of materials for their optical properties, a goal which is scarcely achieved in the literature. Hence, in order to try to understand the relationship between bond interactions and optoelectronic properties, the electron density topology has been investigated using Bader's quantum theory of atoms in molecules (QTAIM).[15] The investigation of the structure-properties relationship in the Cu-Sb-S compounds has never been done to date. Although the optical properties have already been published for $CuSbS_2$,[3,17,18] Cu_3SbS_3[3] and Cu_3SbS_4,[3,19] we have reinvestigated these properties for the three compounds with the same procedure, with the aim of studying the relation between the QTAIM-based bonding features and the optical properties. The analysis of the bonding features in $CuSbS_2$, Cu_3SbS_3 and Cu_3SbS_4 reveals that Cu-S and Sb-S bonds in Cu_3SbS_4 are seemingly less polarizable, which seems to induce a smaller absorption coefficient for this material.

Computational Details

First principles density functional theory calculations using the FP-LAPW method based on Kohn–Sham equations were carried out using the WIEN2k package.[20] The structural optimizations were performed using the generalized gradient approximation (GGA) with the Perdew, Burke, and Ernzerhof (PBE) functionals[21] as implemented in the WIEN2k package. As the Tran-Blaha-modified Becke-Johnson (TB-mBJ) potential allows for estimating band gap energies more accurately, it was used to calculate electron band structures and density of states.[22–24] Unfortunately, since the TB-mBJ functional gave the wrong band gap energy for Cu_3SbS_4, the hybrid functional of Heyd, Scuseria, and Ernzerhof (HSE06) was utilized for this compound.[25] The core-valence electron separation, which was set to − 6.0 eV, is defined as follows: Cu [Ar] $3p^6$ $3d^{10}$ $4s^1$, Sb [Kr] $4d^{10}$ $5s^2$ $5p^3$, and S [Ne] $3s^2$ $4p^4$. The structural optimization was performed by calculating the total energy (in Ry) with respect to crystal volume, *b*/*a*, and *c*/*a* ratio in proper sequence, and full structural relaxation was carried out until the total residual forces on all atoms was less than 2 mRy per Bohr. The optimized volumes and cell parameters were obtained from fitting curves against the Birch–Murnaghan equation of state:

$$E(V) = E_o + \left(\frac{9V_o}{16}\right)\left(\frac{B}{4703.6}\right)\left(\eta^2 - 1\right)^3 B_p + \left(\eta^2 - 1\right)^2\left(6 - 4\eta^2\right), \tag{1}$$

$$\eta = \left(\frac{V_o}{V}\right)^{\frac{1}{3}}, \tag{2}$$

where V_0, and V are the initial and distorted volumes, B is the bulk modulus, and B_P is the derivative of bulk modulus with respect to pressure.

The convergence parameter $R_{MT}K_{max}$ was set to 7, where R_{mt} is the radius of the smallest sphere and K_{max} is a maximum wave vector. The charge density was obtained up to G_{max}=14 $(a.u.)^{-1}$. For the TB-mBJ calculations, the Brillouin zone was sampled with a mesh of 1000 k-points. For hybrid calculations, a $6 \times 6 \times 6$ grid of 30 k-points was used. A $16 \times 16 \times 16$ k-points grid (4096 k-points in the full Brillouin zone) was used for optical calculations.

The optical properties of the Cu-Sb-S compounds were calculated based on their response to electromagnetic perturbations as implemented in the Wien2k OPTIC module.[26] The frequency-dependent complex dielectric function was determined as $\varepsilon(\omega) = \varepsilon_1(\omega) + i\varepsilon_2(\omega)$, where ω is the photon frequency. The imaginary (absorptive) part of dielectric function $\varepsilon_2(\omega)$ is calculated using the following momentum matrix elements between the valence and conduction wave functions:

$$\varepsilon_2(\omega) = \frac{e^2\hbar}{\pi m^2\omega^2}\sum_{v,c}\int_{BZ}\left|M_{cv}(k)\right|^2\delta\left\{\omega_{cv}(k)\omega\right\}d^3k. \tag{3}$$

The real (dispersive) part of the dielectric function $\varepsilon_1(\omega)$ and the absorption coefficient $\alpha(\omega)$ were calculated by Kramers–Kronig transformation as

$$\varepsilon_1(\omega) = 1 + \frac{2}{\pi} P \int_0^{\infty} \frac{\omega' \varepsilon_2(\omega')}{\omega'^2 - \omega^2} \mathrm{d}\omega', \tag{4}$$

$$\alpha(\omega) = \sqrt{2}\omega \left[\sqrt{\varepsilon_1(\omega)^2 + \varepsilon_2(\omega)^2} - \varepsilon_1(\omega) \right]^{\frac{1}{2}}, \tag{5}$$

where P is the momentum operator. The extinction coefficient $k(\omega)$, energy loss $L(\omega)$, and refractive index $n(\omega)$ were calculated using real and imaginary parts of the dielectric function as

$$k(\omega) = \left[\frac{\sqrt{\varepsilon_1^2(\omega) + \varepsilon_2^2(\omega)}}{2} - \frac{\varepsilon_1(\omega)}{2} \right]^{\frac{1}{2}}, \tag{6}$$

$$L(\omega) = \frac{\varepsilon_2(\omega)}{\varepsilon_1(\omega)^2 + \varepsilon_2(\omega)^2}, \tag{7}$$

$$n(\omega) = \left[\frac{\varepsilon_1(\omega)}{2} + \frac{\sqrt{\varepsilon_1^2(\omega) + \varepsilon_2^2(\omega)}}{2} \right]^{\frac{1}{2}}, \tag{8}$$

The reflectivity was calculated by the following equation:

$$R(\omega) = \frac{(n(\omega) - 1)^2 + k(\omega)^2}{(n(\omega) + 1)^2 + k(\omega)^2}. \tag{9}$$

The real-space analysis of the quantum chemical interactions was carried out using the Critic2 program.[27]

Results and Discussion

Crystal Structures of the Cu-Sb-S System Compounds

The crystal structure of $Cu^{I}Sb^{III}S^{-II}$ ($CuSbS_2$, chalcostibite) is composed of square pyramidal SbS_5 units, which share their edges to form continuous SbS_2 units aligned with the b axis. The SbS_2 units are regularly separated by CuS_4 tetrahedra. Thus, the bases of the square pyramidal units are lined up to face one another and the Sb electron lone pair points towards the void separating the SbS_5 units (Fig. 1a). The $Cu^{I}Sb^{III}S^{-II}$ (Cu_3SbS_3) has a skinnerite structure and derives from the wittichenite structure. The Cu atoms are in nearly trigonal planar coordination with S atoms, the Sb atom is trigonally coordinated by S, and S is tetrahedrally coordinated by three Cu atoms and one Sb atom. As can be seen in Fig. 1b, there are different crystallographic positions for both Cu and Sb atoms. The crystal structure of $Cu^{I}Sb^{III}S^{-II}$ (Cu_3SbS_4, famatinite) derives from the zinc blende structure, which is characterized by S atoms lying at the nodes of a face-centred cubic lattice and Cu or Sb atoms located in the tetrahedral sites and forming MS_5 units. The Cu atoms are classified as Cu1 and Cu2, which occupy Wyckoff 2b and 4d positions, while Sb and S atoms occupy 2a and 8i positions, respectively (Fig. 1c). Thus, two types of Cu-S bond and one type of Sb-S bond can be distinguished. Table I gathers

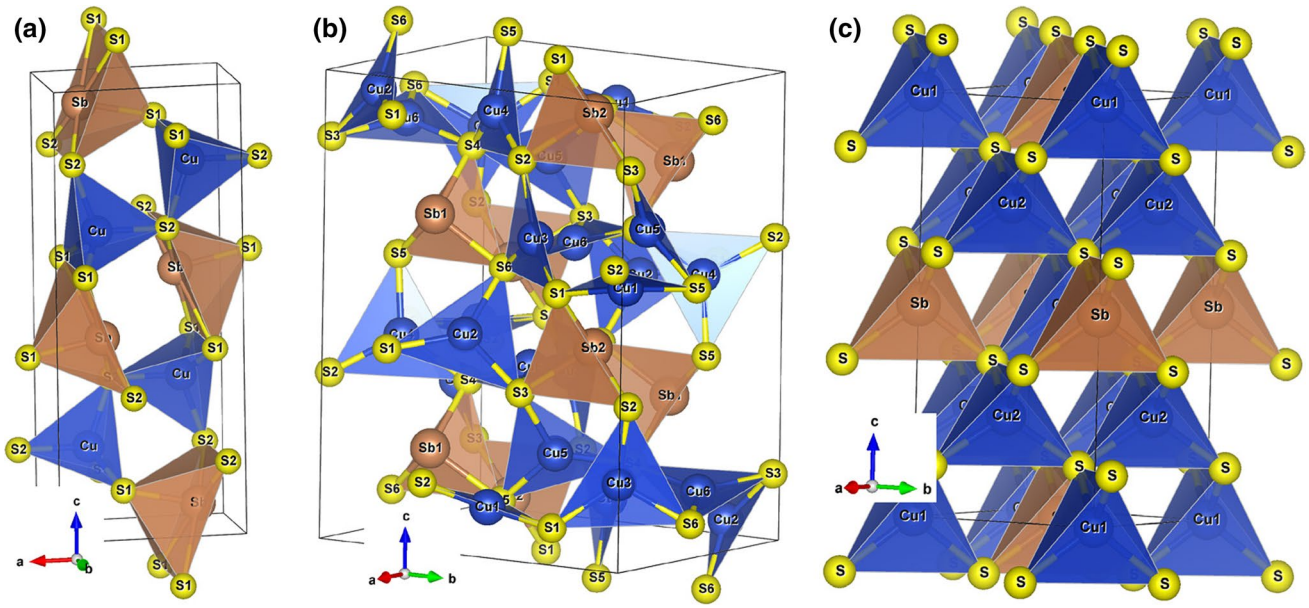

Fig. 1. Optimized crystal of Cu-Sb-S structures. (a) $CuSbS_2$, (b) Cu_3SbS_3 and (c) Cu_3SbS_4.

the lattice constants calculated in this work with the PBE functional for $CuSbS_2$, Cu_3SbS_3, and Cu_3SbS_4 together with the experimental constants reported in the literature. There is a slight overestimation of the lattice parameters (< 2 %) for $CuSbS_2$ and Cu_3SbS_3 compounds, which is quite reasonable for structural results. Further, the Cu_3SbS_4 structure has been optimized with the HSE06 hybrid functional, which leads to better agreement with experimental cell parameters than the PBE functional.

Band Structure of Cu-Sb-S system Compounds

To understand the electronic properties of the Cu-Sb-S compounds, the band structures and the density of states (DOS) were calculated using the PBE and TB-mBJ functionals, as well as the HSE06 functional in the particular case of the Cu_3SbS_4 compound. At first, the band structures of $CuSbS_2$, Cu_3SbS_3, and Cu_3SbS_4 were calculated with the PBE functional along the high symmetry directions in the Brillouin zone (BZ) (Fig. S1). As the modified TB-mBJ potential allows for estimating band gap energies more accurately, the band structures of the Cu-Sb-S compounds were estimated with this potential, the results of which are illustrated in Fig. 2 and Fig. S2. However, the TB-mBJ functional fails to estimate properly the band structure of Cu_3SbS_4 compound (wrong band gap). Thus, the HSE06 functional was used (Fig. 2c). The dashed horizontal line represents the position of the Fermi energy level (E_F). The values of the band gaps E_g were estimated from the energy difference between the conduction band minimum (CBM) and the valence band maximum (VBM), and the data are gathered in Table II.

It is found that the value of band gaps calculated using PBE is underestimated in comparison with experimental values. Furthermore, a closed energy gap calculated with PBE and TB-mBJ around the Fermi level is observed for Cu_3SbS_4 indicating semi-metallic behaviour. With the TB-mBJ potential, the band structure of $CuSbS_2$ shows a VBM located at the Γ-point and a CBM located between the R- and X-points. An indirect band gap of 1.18 eV is then observed, which agrees with the indirect band gap values experimentally reported (Table II). Interestingly, the difference between the lowest direct band gap and fundamental indirect band gap is about 0.1 eV; thus, a strong optical absorption might occur at such energy.[33] Theoretical investigations [3,16–18,28] also found an indirect energy band gap. Assuming from experiment that the band gap is indirect and located in the range 1.0–1.2 eV (Table II), the value reported in Ref. 3 is likely overestimated due to the use of the HSE06 functional. We observe a similar result in Refs 17 and 28. As for Ref. 16 that reports a band gap of 1.28 eV with the TB-mBJ (1.18 eV from our work), a close look to the band structure shows that the conduction band minimum energy is located slightly below 1.2 eV (Fig. 1a of Ref. 16). Hence, a mistyping is not excluded.

The band structure of Cu_3SbS_3 shows that the valence band bears two maxima located at the Γ-point and X-point and that the conduction band bears two minima located at the Γ-point and also the X-point. A direct band gap is observed with a value of 1.28 eV, which is 0.12 eV to 0.59 eV lower than the experimental values (Table II). Furthermore, a flat conduction band bottom is observed. Thus, a strong optical absorption is expected in the Cu_3SbS_3 compound. Considering the wide range of experimental data reporting on the band gap energy of Cu_3SbS_3 (0.93–1.87 eV) the quality of our estimate is difficult to assess. Unsurprisingly, the HSE06 functional[3] yields larger value (1.5 eV) than the TB-mBJ potential.

The band structure of Cu_3SbS_4 exhibits VBM and CBM at Γ-point leading to a direct band gap with a value of 1.0 eV, as estimated by the HSE06 functional, which agrees well with both the direct and indirect energy band gap values determined by experiments. By contrast, theoretical

Table I. Calculated lattice constants compared with experimental literature data

Compound	Crystal structure	Space group	Lattice constants						Method	Ref.
			a (pm)	b (pm)	c (pm)	α (°)	β (°)	γ (°)		
$CuSbS_2$ chalcostibite	Orthorhombic	Pnma (62)	611.8	385.3	1457.3	90	90	90	PBE	This work
	Orthorhombic	Pnma (62)	602.4	378.6	1470.1	90	90	90	Exp.	2
	Orthorhombic	Pnma (62)	601.6	379.7	1449.9	90	90	90	Exp.	28
	Orthorhombic	Pnma (62)	602.0	379.0	1449.0	90	90	90	Exp.	29
Cu_3SbS_3 skinnerite	monoclinic	P121/c (14)	804.5	1034.1	1340.1	90	90.4	90	PBE	This work
	monoclinic	P121/c (14)	780.8	1023.3	1326.8	90	90.4	90	Exp.	29
	monoclinic	P121/c (14)	784.6	1024.7	1325.3	90	90.4	90	Exp.	30
Cu_3SbS_4 famatinite	Tetragonal	I-42m (121)	549.2	549.2	1085.7	90	90	90	PBE	This work
		I-42m (121)	544.7	544.7	1081.7	90	90	90	HSE06	This work
	Tetragonal	I-42m (121)	539.1	539.1	1087.0	90	90	90	Exp.	31
	Tetragonal	I-42m (121)	539.0	539.0	1075.0	90	90	90	Exp.	32

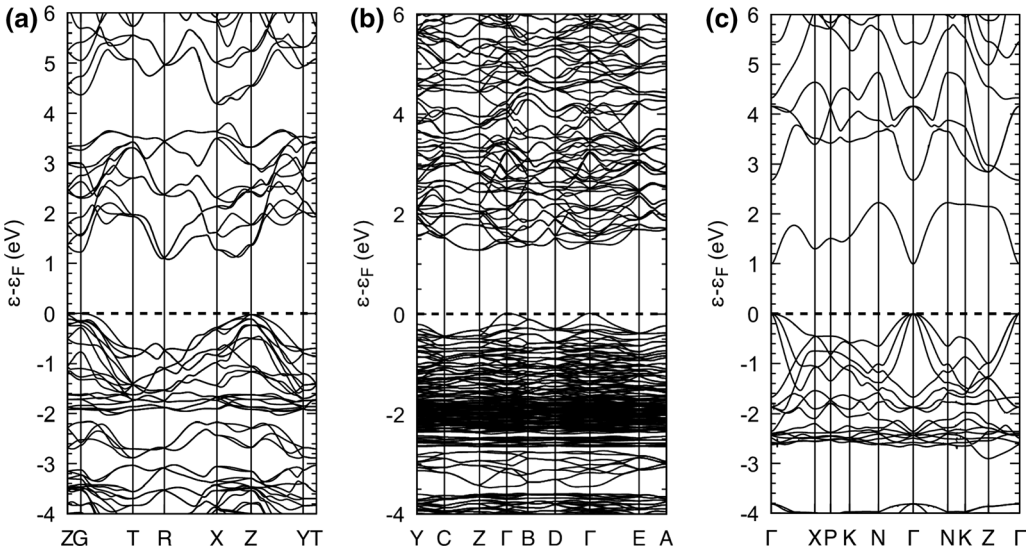

Fig. 2 Band structures of $CuSbS_2$ (a) and Cu_3SbS_3 (b) crystals calculated with the TB-mBJ potential functional, and Cu_3SbS_4 (c) calculated with the hybrid HSE06 functional.

works[3,19,32] report quite different band gap values from ours, though with the same hybrid functional. Ramasamy et al.[3] indeed notice their surprisingly high band gap value of 2.5 eV, but do not provide hints to explain this result. On the contrary, Li et al.[19] calculated quite low direct band gap energy of 0.39 eV at the Γ-point. We have no explanation for this difference. In between lies the value 0.85 eV found by Chen et al.[32] The smaller value compared to ours could be explained by the spin-orbit coupling that is accounted for in their calculations.

The energetic distributions of the electronic states for $CuSbS_2$ and Cu_3SbS_3 compounds have been investigated by calculating the density of states with the TB-mBJ potential functional, and for the Cu_3SbS_4 compound by the hybrid HSE06 functional. Figure 3 shows the atom-projected and orbital-projected density of states (aDOS and oDOS) for Cu-Sb-S compounds in the energy range from −7 eV to 7 eV. The aDOS contains different energy regions and is contributed by each atom of the crystal system (Fig. 3a, c, and e), while the oDOS represents the contribution of different orbital states of the interconnected atoms (Fig. 3b, d, and f). The fully occupied d orbitals of Sb are not considered in our study. For $CuSbS_2$, the region [− 6.0; − 1.7] eV is mainly contributed by Cu and S atoms and slightly by Sb atoms. These contributions correspond to Cu-3d and S-3p, and to a lesser extent by Sb-5p/5s, particularly in the region [− 2.9; − 1.97] eV. The regions [− 1.7; 0.0] eV and [1.0; 3.8] eV are mainly contributed by Cu and S with a predominance of Cu-3d orbitals and S-3p orbitals hybridization and by Sb and S atoms corresponding to mixing of Sb-5p and S-3p orbitals, respectively. The region [4.35; 7.0] eV mainly contains the Cu, Sb, and S atoms contributions, which correspond to Cu-4s, S-3p, and Sb-5p orbitals interactions. For Cu_3SbS_3, four regions can be observed, namely [− 6.16; − 2.52] eV contributed by Cu, Sb and S atoms (Cu-3d, S-3p and small contribution of Sb-5p/5s), [− 2.52; 0.0] eV mainly contributed by Cu atoms and a very small contribution of S atoms (Cu-3d and S-3p), [1.18; 4.0] eV mainly contributed by Sb and S atoms (Sb-5p and S-3p orbitals) and [4.0; 7.0] eV contributed by Cu, Sb and S atoms (Cu-4s, S-3p and Sb-5p orbitals). The DOS of the Cu_3SbS_4 compound can be divided into five regions separated by energy gaps. These regions are [− 7.32; − 4.34] eV, which is contributed by Cu, S and to a lesser extent by Sb (Cu-3d, S-3p, and Sb-5p orbital at higher energy (>− 5. 98 eV)), [− 3.47; − 0.56] eV, which is mainly contributed by Cu and to a lesser extent by S (Cu-3d and S-3p orbitals interactions), [0.7; 1.65] eV, which is composed of Cu, Sb and S atoms (Sb-5s and S-3p and small contribution of Cu-3d orbitals), [2.2; 4.03] eV, which is mainly assigned to Sb and a small contribution of S atoms (Sb-5p and S-3p orbitals) and [4.2; 7.0] eV, which is attributed to Cu, Sb and S atoms (Cu-4s, Sb-5p, and S-3p orbitals interactions). It is found that the DOS peaks located in the vicinity of the valence band maximum of $CuSbS_2$, Cu_3SbS_3, and Cu_3SbS_4 are predominated by a strong Cu-3d and S-3p orbitals hybridization. The conduction band of both $CuSbS_2$ and Cu_3SbS_3 is mainly contributed by mixing of Sb-5p and S-3p orbital, while the conduction band of Cu_3SbS_4 is dominated by mixing of Sb-5s and S-3p orbitals. As the oxidation state of copper is +I in all the Cu-Sb-S compounds (Cu^+, $3d^{10}$), the $3d^{10}$ orbitals in the valence band are fully occupied; therefore, a very small contribution of Cu-3d orbital states occurs in the conduction band. The contribution of Sb-5s orbital is very small in the VBM

Table II. Calculated band gaps of the Cu-Sb-S compounds compared with the literature data

Chemical compound	Transition type	E_g (eV)	Method	Ref.
$CuSbS_2$ (Chalcostibite)	Direct	1.4	Exp. (Transmission)	2
	Indirect	1.1	Exp. (Absorbance)	3
	Indirect	1.6	Calc. (DFT, HSE06)	3
	Direct	1.2	Exp. (Reflectance)	29
	Indirect	1.0	Exp. (Reflectance)	29
	N/A	1.53	Exp. (Absorbance)	34
	Direct	1.58	Exp. (Absorbance)	35
	Indirect	1.28	Calc. (DFT, TB-mBJ)	16
	Indirect	1.72	Calc. (DFT, HSE06)	17
	Indirect	0.79	Calc. (DFT, PBE)	17
	Indirect	1.16	Calc. (DFT, HSE06)	18
	Indirect	0.77	Calc. (DFT, PBE)	18
	Indirect	1.69	Calc. (DFT, HSE06)	28
	Indirect	0.9	Calc. (DFT, PBE)	28
	Indirect	0.86	Calc. (DFT, PBE)	This work
	Indirect	1.18	Calc. (DFT, TB-mBJ)	This work
Cu_3SbS_3 (Skinnerite)	Direct	1.4	Exp. (Absorbance)	3
	Direct	1.5	Calc. (DFT, HSE06)	3
	Direct	1.85	Exp. (Reflectance)	29
	Indirect	1.52	Exp. (Reflectance)	29
	Direct	1.46	Exp. (Reflectance)	30
	N/A	0.93	Exp. (Absorbance)	34
	Direct	1.6	Exp. (Reflectance)	36
	Direct	1.87	Exp. (Absorbance)	37
	Indirect	1.07	Calc. (DFT, PBE)	This work
	Direct	1.28	Calc. (DFT, TB-mBJ)	This work
Cu_3SbS_4 (Famatinite)	Indirect	1.2	Exp. (Absorbance)	3
	Indirect	2.5	Calc. (DFT, HSE06)	3
		0.85	Calc. (DFT, HSE06)	32
		0.58	Calc. (quasi-particle self-consistent GW)	17
	Direct	0.9	Exp. (Absorbance)	38
	N/A	1.72	Exp (Absorbance)	34
	Direct	0.82	Exp. (Reflectance)	39
		0.47	Exp. (Absorbance)	40
	Indirect	1.0	Exp. (Absorbance)	41
	Direct	0.89	Exp. (Ultraviolet photoelectron spectroscopy)	42
	Direct	0.39	Calc. (DFT, HSE06)	19
		0.0	Calc. (DFT, PBE)	This work
		0.0	Calc. (DFT, TB-mBJ)	This work
	Direct	1.0	Calc. (DFT, HSE06)	This work

region of $CuSbS_2$ and Cu_3SbS_3, thus the Sb 5s electrons have weak interaction with S-3p and become chemically inert as lone-pair electrons. As it was observed in PbS,[43] the crystal systems in which $CuSbS_2$, and Cu_3SbS_3 crystallize, namely orthorhombic and monoclinic, are dictated by this electron lone pair, which necessitates a distortion of the crystal lattice to be energetically stable. Despite having an inert effect on chemical bonds, this electron lone pair has a stereochemical effect on the crystal structure and is only involved in van der Waals interactions. By contrast, in the case of Cu_3SbS_4, ($Cu^{I}Sb^{V}S^{-II}$) there is no pure Sb-5s orbital accommodating electrons, and the atoms are connected via covalent bonds to form Chalcopyrite tetrahedral structure. Therefore, the Cu-Sb-S compounds offer various bonding properties that deserve investigation through the topological analysis of the electron density.

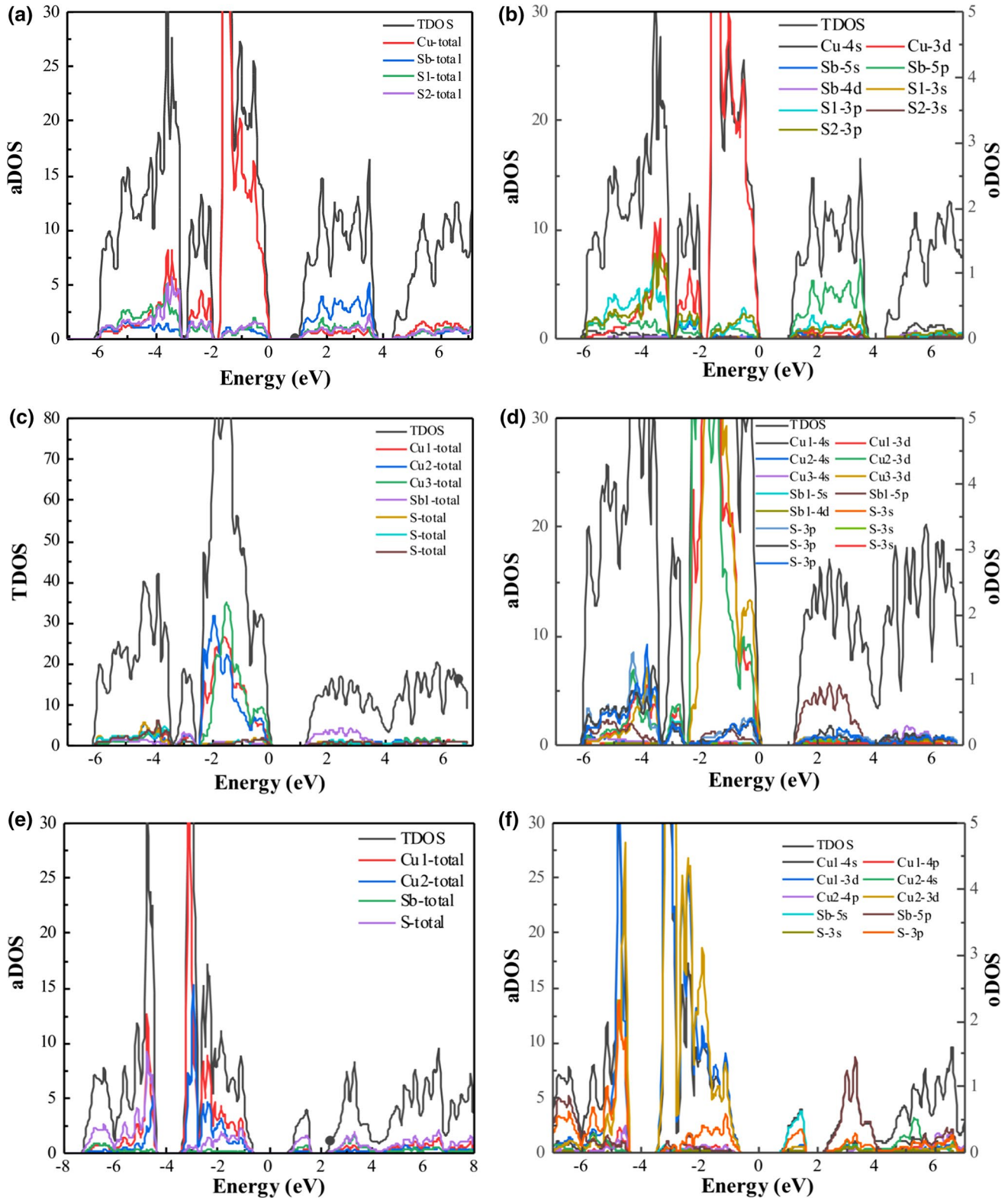

Fig. 3 Atom-projected density of states (aDOS) and orbital-projected density of states (oDOS) for $CuSbS_2$ (a, and b) and Cu_3SbS_3 (c and d) calculated with the TB-mBJ potential functional, and Cu_3SbS_4 (e, and f) calculated with the HSE06 functional. The unit of aDOS and oDOS is states/eV. TDOS, total density of states (in states/eV) that corresponds to summed atomic DOS (left-axis scale).

Electron Density Topological Properties of the Cu-Sb-S System Compounds

Since the knowledge of structure-property relationship is still limited, investigating quantum-mechanical atomic and molecular interactions in solid crystals is relevant in view of material design for the targeted application. In this context, the investigation of electron density in real space within solids has been studied by the quantum theory of atoms in molecules (QTAIM [15]) using the Critic2 program. The calculated electron density Laplacians of $CuSbS_2$, Cu_3SbS_3, and Cu_3SbS_4 are depicted in Fig. 4a-d, respectively. The symbols b, r, and c represent bond, ring, and cage critical points, respectively, as described in the QTAIM theory. Bond length, bond angle, electron density (ρ_{BCP}), electron density Laplacian ($\nabla^2\rho_{BCP}$), ellipticity, and local potential (V_{BCP}), kinetic (G_{BCP}), and total energy (H_{BCP}) densities at bond critical points (BCP) extracted from the Critic2 program outputs are gathered in Table S1. The relation between electron density Laplacian, kinetic energy G_{BCP}, and potential energy V_{BCP} densities at BCP is given by

$$\frac{\hbar^2}{4m}\nabla^2\rho_{BCP} = 2G_{BCP} + V_{BCP}, \quad (10)$$

and the variation of bond degree (BD = H_{BCP}/ρ_{BCP}) versus $|V_{BCP}|/G_{BCP}$ ratio can be used to distinguish bonding types,[44] Figure 4e shows these characteristics for $CuSbS_2$, Cu_3SbS_3, and Cu_3SbS_4. A linear evolution is observed with a correlation coefficient R^2 of 0.904, 0.993, and 0.867, respectively. Three and 17 different Cu-S bonds can be observed in $CuSbS_2$ and Cu_3SbS_3, respectively (see Table S1). The longest Cu-S bond in each Cu-Sb-S structure is distinguished with an asterisk sign (*) in Fig. 4e. Although the electron density Laplacian (Fig. 4a-d) for Cu-S bonds differs from one structure to another, the kinetic energies per electron at the bond critical point (G_{BCP}/ρ_{BCP}), which are related to the polarizability of the charge distribution,[44] are almost the same (comprised between 0.82 and 0.87, see Table S1). The best concordance is observed between $CuSbS_2$ and Cu_3SbS_3 (Fig. 4e). Moreover, the local energy densities for $CuSbS_2$ and Cu_3SbS_3 are all very close to one another on the graph. All these results suggest that the Cu-S bonds in $CuSbS_2$, Cu_3SbS_3, and Cu_3SbS_4 have close bonding characteristics, though not strictly the same due to the difference in atom environments.

In agreement with Ref. 44, for similar G_{BCP}/ρ_{BCP} the interatomic distances increase with the absolute value of the bond degree. This is exemplified for the Cu-S bonds in Fig. 4f, though this holds for the Sb-S bonds too. Espinosa et al. classified the bonds into three categories based on the $|V_{BCP}|/G_{BCP}$ ratio and bond degree (BD) H_{BCP}/ρ_{BCP} [45]: Pure closed-shell (CS) including ionic bond, hydrogen bond, and van der Waals interactions ($|V_{BCP}|/G_{BCP} < 1$), pure shared-shell (SS) including covalent and polar bonds ($|V_{BCP}|/G_{BCP} > 2$), and bonds belonging to the transit region with positive Laplacian and negative total energy density ($1 < |V_{BCP}|/G_{BCP} < 2$). It is found that the Cu-S and Sb-S bonds for Cu-Sb-S structures lie in the transit zone, between the typical ionic and covalent bonds. Both the Cu-S and Sb-S bonds bare negative H_{BCP}/ρ_{BCP} values indicating that the potential energy density dominate the total energy and that the electrons at the bond critical point tend to exert pressure on the neighbouring electron cloud. As the Cu-S bonds locate in the mid-range of H_{BCP}/ρ_{BCP} values in the diagram (Fig.4e), one can state that these bonds are ionic in nature with small covalent contribution. By contrast, the Sb-S bonds bare larger $|V|/G$ ratio with large, negative H_{BCP}/ρ_{BCP} values, hence these bonds are more covalent in nature than the Cu-S bonds. These observations are confirmed by the positive values of the electron density Laplacian $\nabla^2\rho_{BCP}$ at the bond critical points that evidence the tendency of electrons to escape from the bonding region. Indeed, for the Sb-S bonds $\nabla^2\rho_{BCP}$ amounts to around 5 electrons $Å^{-5}$ for both $CuSbS_2$ and Cu_3SbS_3 and 3.7 electrons $Å^{-5}$ for Cu_3SbS_4 , whereas for the Cu-S bonds it amounts to about 14 electrons $Å^{-5}$ and 14–15 electrons $Å^{-5}$ for both $CuSbS_2$ and Cu_3SbS_3 and 13–14 electrons $Å^{-5}$ for Cu_3SbS_4. The Sb-Sb and Cu-Cu bonds for $CuSbS_2$ and Cu_3SbS_3, respectively, lie close to the point ($|V_{BCP}|/G_{BCP}=1$, $H_{BCP}/\rho_{BCP}=0$), which correspond to non-localized interactions (weak dipole-dipole interactions such as for van der Waals). By contrast, Cu_3SbS_4 does not bare such interactions. These data indicate that the bonding network in Cu_3SbS_4 is more covalent, hence seemingly less polarizable, than that in $CuSbS_2$ and Cu_3SbS_3.

The accumulation of electron density at BCP is generally increased along bond path as the bond length decreases. This means large overlapping of electron clouds and increased refractive index of the materials. The optical properties of the semiconductor materials under incident photons depend on the electron transition from valence band maximum to empty conduction band minimum, attributed in the compounds of interest to mixing of Cu-3d/S-3p and Sb-5p or Sb-5s/S-3p, respectively. The Sb-S bonds with a large bond degree revealed a high absorption coefficient ($> 10^4$ cm^{-1}) of Cu-Sb-S materials near the Fermi level. These results should lead to a lower band gap of $CuSbS_2$ compared to that of Cu_3SbS_4. However, the presence of empty Sb-5s orbital in the conduction band causes a Sb-5s/S-3p hybridization in the case of Cu_3SbS_4, which confers it a lower band gap than expected, leading to a reversed band gap order between $CuSbS_2$ and Cu_3SbS_4 as shown in Figs. 2 and 3.

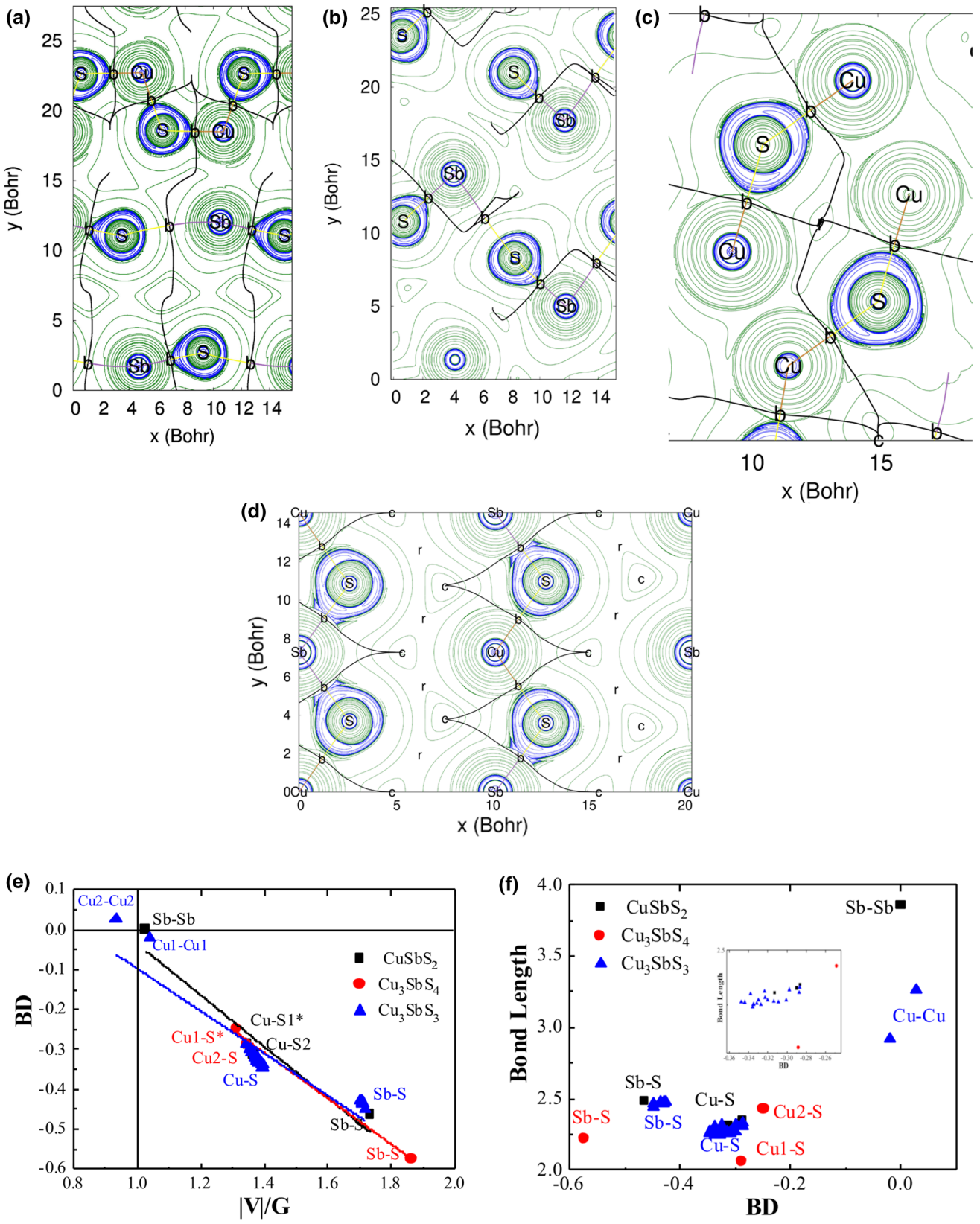

Fig. 4 Electron density Laplacian of (a) $CuSbS_2$ (plane (005)), (b) Cu_3SbS_3 (plane (040)), (c) Cu_3SbS_3 (plane (49-1)) and (d) Cu_3SbS_4 (plane (110)). (e) Bond degree (BD=H_{BCP}/ρ_{BCP}) versus $|V_{BCP}|/G_{BCP}$. (*) represents the longest bond length for each pair. (f) Relation between bond length and bond degree at BCPs for Cu-Sb-S system compounds. b, r and c stand for bond, ring and cage critical points. Bond degree in Hartree electron^{-1}; Bond lengths in Å.

Optical Properties of Cu-Sb-S System Compounds

The valence band maximum (VBM) of Cu-Sb-S structures is mainly due to the mixing of Cu-3d and S-3p, which can stabilize the holes and provides high mobility Cu/S framework paths. The optical properties of $CuSbS_2$ and Cu_3SbS_3 were calculated using the TB-mBJ potential functional, while those of Cu_3SbS_4 were calculated using the HSE06 functional. The refractive index, extinction coefficient, absorption coefficient, and reflectivity were determined by utilizing the calculated dielectric function as described in the computational section. For Cu_3SbS_4 with a tetragonal structure, the optical functions are analysed along two directions, namely *xx* and *zz*, while for $CuSbS_2$ and Cu_3SbS_3 with orthorhombic and monoclinic structures the optical properties are analysed according to the three diagonal components *xx*, *yy*, and *zz*. The dielectric function $\varepsilon(\omega)$ characterizes the collective excitations close to the Fermi-level and depends strongly on the band structure.[46] The calculated dielectric functions for $CuSbS_2$, Cu_3SbS_3, and Cu_3SbS_4 are depicted in Fig. 5, the real parts $\varepsilon_1(\omega)$ of which are shown in Fig. 5a, c and e and the imaginary parts $\varepsilon_2(\omega)$ of which are shown in Fig. 5b, d and f. The maximum peak values of $\varepsilon_1(\omega)$ for $CuSbS_2$ (Fig. 5a), Cu_3SbS_3 (Fig. 5c), and Cu_3SbS_4 (Fig. 5e) are in fair agreement with those reported in the literature (Ref 16 for $CuSbS_2$ and Ref 19 for Cu_3SbS_4). $\varepsilon_1(\omega)$ becomes negative above a certain photon energy: about 6 eV for the $CuSbS_2$ and Cu_3SbS_3 compounds, and about 8 eV for Cu_3SbS_4. This indicates that the Cu-Sb-S materials have a metallic character above these photon energy thresholds.[16] At zero frequency limit ($\omega = 0$), $\varepsilon_1(\omega)$ gives the static dielectric permittivity. Lower static dielectric permittivity values have been obtained for Cu_3SbS_4 indicating lower polarizability for this compound. This result agrees with the weighted average G_{BCP}/ρ_{BCP} values (Table S1) since higher G_{BCP}/ρ_{BCP} corresponds to lower polarizability.[44] According to the Penn model [47] $\varepsilon_1(0)$ is defined as $\varepsilon_1(0) \approx 1 + (\hbar\omega/E_g)^2$, where $\hbar\omega$ is the plasma energy. Hence, the band gap of the Cu-Sb-S materials should increase when going from Cu_3SbS_4 to $CuSbS_2$ and to Cu_3SbS_3. This is supported by our band gap calculations (see "Band Structure of Cu-Sb-S system Compounds" Section). Further, the edge of the optical absorption that can be seen on Fig. 5b, d and f is located at about 1.1 eV, 1.2 eV and 1.1 eV for $CuSbS_2$, Cu_3SbS_3 and Cu_3SbS_4, respectively. Although the structures are not cubic, the absorption energy threshold does not depend on the crystal direction. The absorption maxima fall in the domain of the visible light, around 2 eV, making these compounds potentially suitable for optical applications. Nonetheless, the peak maximum of $\varepsilon_2(\omega)$ for Cu_3SbS_4 is significantly lower than that of $CuSbS_2$ and Cu_3SbS_3, evidencing a lower absorption efficiency of Cu_3SbS_4. In addition, along the series $CuSbS_2$, Cu_3SbS_3, Cu_3SbS_4 the decreasing tendency of $\varepsilon_2(\omega)$ values and the shift of the peak maximum towards higher incident energies indicate a decrease of the ability of the Cu-Sb-S compounds to absorb light. Thus, $CuSbS_2$ compound has the highest ability to absorb the incident light although it has indirect band gap.[33] Compared with theoretical data reported

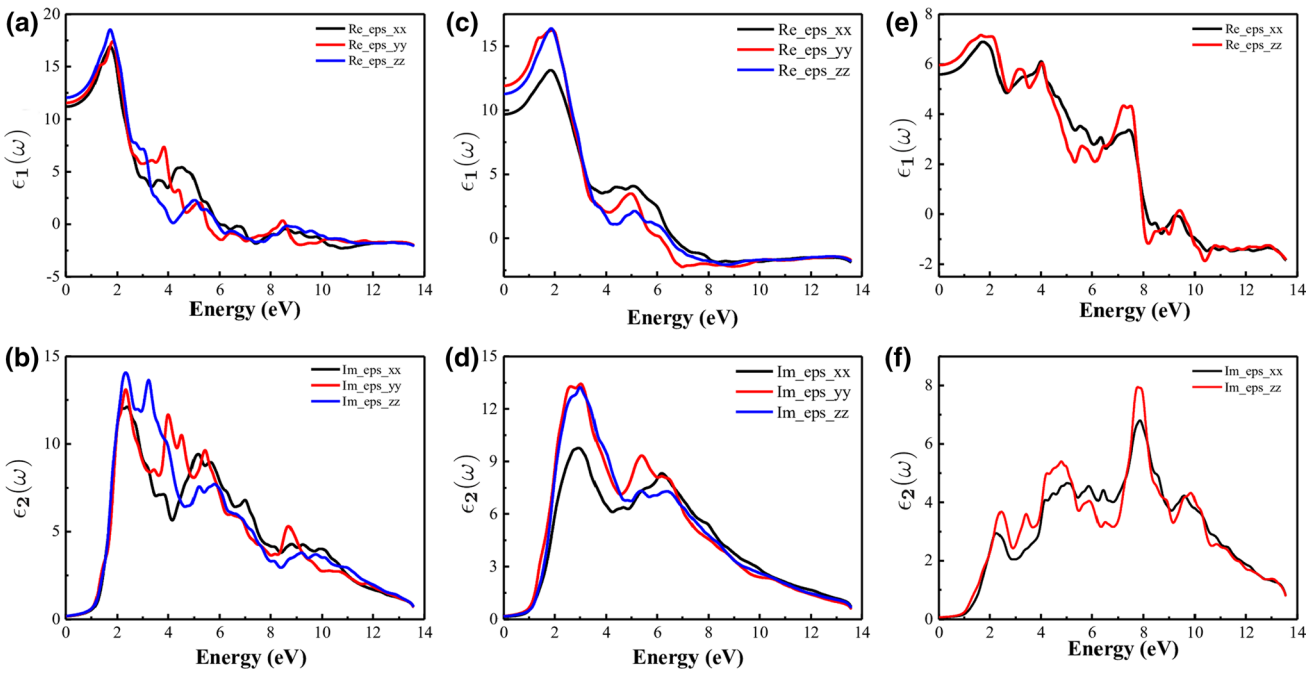

Fig. 5 Real and imaginary dielectric functions of Cu-Sb-S materials: (a, and b) $CuSbS_2$; (c, and d) Cu_3SbS_3; (e, and f) Cu_3SbS_4.

in the literature [16,19] for $CuSbS_2$ and Cu_3SbS_4, the following comments can be made. For $CuSbS_2$ the maximum values of $\varepsilon_2(\omega)$ are in fair agreement with ours, the peak being slightly shifted towards lower photon energies in our case. The agreement is worse for Cu_3SbS_4 as the peak reported by Li et al.[19] is significantly shifted toward lower photon energies. This might be explained by their energy band gap for Cu_3SbS_4 that they found much smaller (0.39 eV) than us (1.0 eV). As the same HSE06 functional is used in both investigations, the origin of this difference is not to be found in the treatment of exchange-correlation, and our structures are the same, hence this discrepancy is difficult to track down. The difference in the energy gaps can also explain the differences observed in the absorption results between our results and those of Ramasamy et al.[3] for Cu_3SbS_4. As they mentioned in their article, the calculated gap is highly overestimated. Again, the same exchange-correlation functional has been used in their work as in ours, which makes it difficult to explain the difference. By contrast for Cu_3SbS_3, both the energy gap and the absorption spectrum calculated in [3] are close to ours.

Comparing with the density of states of the compounds (Fig. 3), the transitions responsible for the peaks at the absorption edge (around 2 eV) in $\varepsilon_2(\omega)$ are mainly Cu-3d to Sb-5p for all three compounds. Higher energy peaks (around 5–6 eV) involve deeper valence states and higher conduction ones (e.g., S-3p to Cu-3d or S-3p to Sb-5p).

The absorption coefficient spectra $\alpha(\omega)$ of $CuSbS_2$, Cu_3SbS_3, and Cu_3SbS_4 are plotted in Fig. 6a, b, and c, respectively. As the photon energy increases the absorption coefficient of these materials increases, showing successive peaks of increasing intensity, which is a typical feature of semiconductors. These absorption peaks correspond to various electronic transitions from the valence band to the conduction one. The band gaps calculated along the *xx*, *yy* and *zz* directions are 1.18 eV, 1.09 eV, and 1.16 eV for $CuSbS_2$, 1.29 eV, 1.30 eV and 1.30 eV for Cu_3SbS_3, and 1.01 eV, 1.01 eV and 1.03 eV for Cu_3SbS_4, respectively. The absorption coefficient increases sharply above 2 eV, except for Cu_3SbS_4 for which the increase is smooth and the first peak is much lower than that of $CuSbS_2$ and Cu_3SbS_3. These observations are coherent with the previous one on the imaginary part of the dielectric function. That the absorption coefficient of Cu_3SbS_4 is smaller than that of the other compounds could make it less suitable for optical usage. This property could however be counteracted by reflectivity,

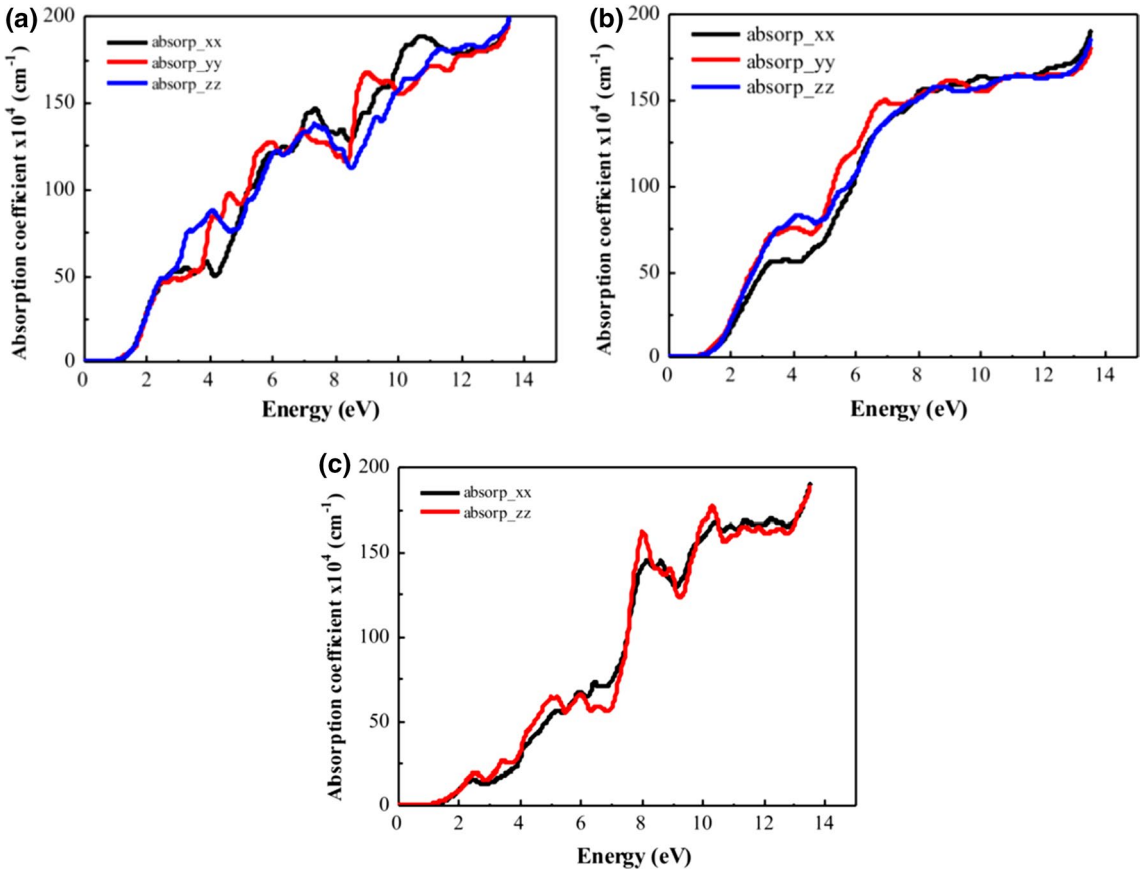

Fig. 6 Absorption coefficient of Cu-Sb-S materials: (a) $CuSbS_2$, (b) Cu_3SbS_3 and (c) Cu_3SbS_4.

which is much larger for Cu_3SbS_4 than for the other compounds (see below).

The relative behaviours of $CuSbS_2$, Cu_3SbS_3 and Cu_3SbS_4 in terms of their absorption coefficient can be explained in the light of the chemical bond analysis (vide supra). Indeed, the Sb-S and Cu-S chemical bonds in Cu_3SbS_4 are more covalent (i.e., more localized electrons and less polarizable electron cloud) than their congeners in $CuSbS_2$ and Cu_3SbS_3, as the $|V|/G$ ratio is larger, the bond degree H_{BCP}/ρ_{BCP} is more negative, and the electron density Laplacian is smaller for Cu_3SbS_4. In addition, there are no weak (van der Waals-like) interactions in Cu_3SbS_4, which could have made the electron cloud more polarizable. Overall, the polarizability of Cu_3SbS_4 is lower, possibly leading to lower absorption coefficient.

Figure 7 shows the variation of the extinction coefficient $k(\omega)$ with photon energy for $CuSbS_2$, Cu_3SbS_3, and Cu_3SbS_4. The evolution of the depicted curves of $k(\omega)$ is fairly close to that of the corresponding imaginary part of the dielectric function. This indicates high efficiency of the $CuSbS_2$ and Cu_3SbS_3 compounds and to a lesser extent of the Cu_3SbS_4 one for photovoltaic applications due to absorption of the most intense part of the sun radiation. The calculated energy loss $L(\omega)$ for $CuSbS_2$, Cu_3SbS_3, and Cu_3SbS_4 are shown in Fig. 8a, b, and c, respectively. The energy loss curves, which relate to the energy lost by fast-moving electrons in the material, should provide information about the plasmon energies $\hbar\omega_p$ as the $\hbar\omega_p$ values correspond to the maxima of the $L(\omega)$ curves and coincide with both the crossing point of $\varepsilon_1(\omega)$ with the x-axis with positive slope and $\varepsilon_2(\omega)$ having negative slope.[48] Although the $L(\omega)$ curves are difficult to interpret due to their complex shapes, it appears that for $CuSbS_2$ and Cu_3SbS_4 the maxima of $L(\omega)$ at 8.54 eV and 9.27 eV, respectively, coincide with the features described for $\varepsilon_1(\omega)$ and $\varepsilon_2(\omega)$ and should hence correspond to the plasmon energies of these compounds. In addition, the maxima of the energy loss function provide information about strain in solid materials.[49] Thus, Cu_3SbS_3 and Cu_3SbS_4 compounds offer better relative stability for photovoltaic applications compared to $CuSbS_2$.

Figure 9 shows the reflectivity $R(\omega)$ of $CuSbS_2$, Cu_3SbS_3, and Cu_3SbS_4 with respect to photon energy. The features of $R(\omega)$ show that a sharp decrease appears at 8.54 eV and 9.27 eV for $CuSbS_2$ and Cu_3SbS_4, respectively, which can be assigned to the plasmon energies. Above 12 eV, a sharp increase of the curves is observed, which

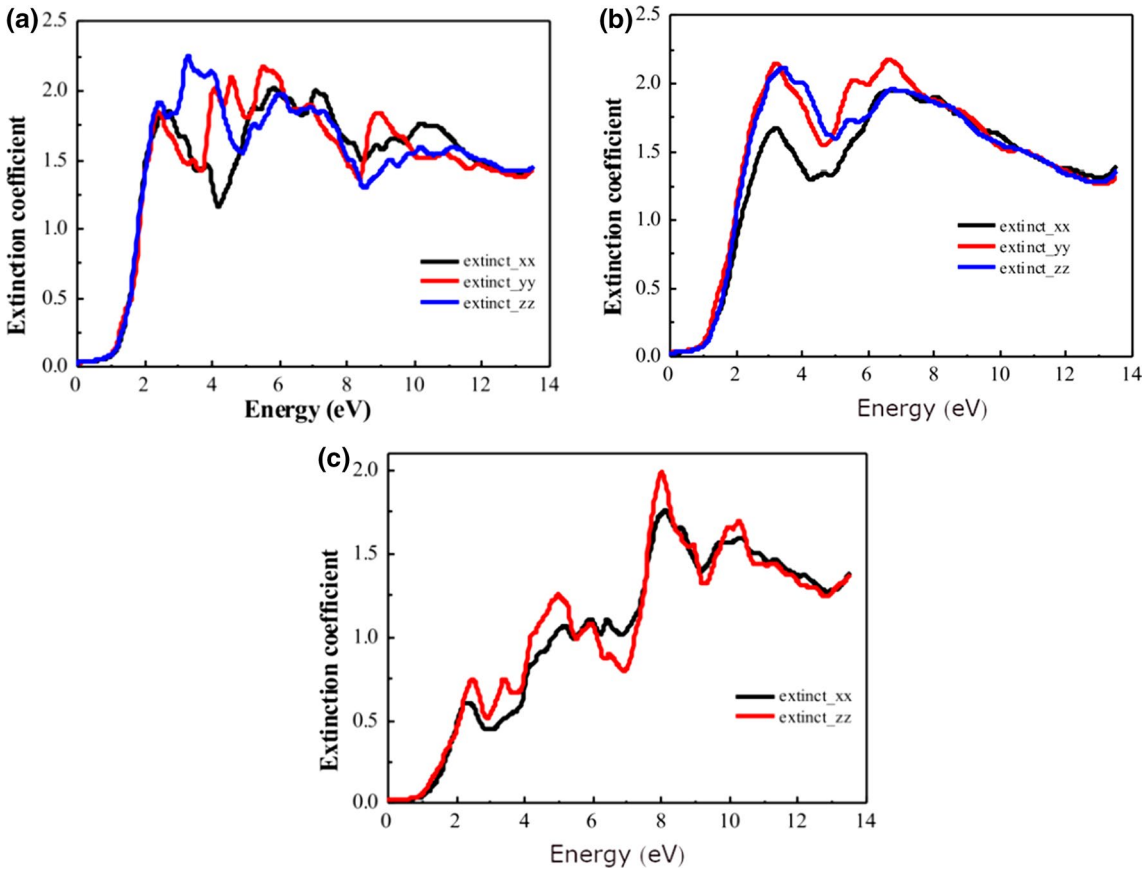

Fig. 7 Extinction coefficient of Cu-Sb-S materials: (a) $CuSbS_2$, (b) Cu_3SbS_3 and (c) Cu_3SbS_4.

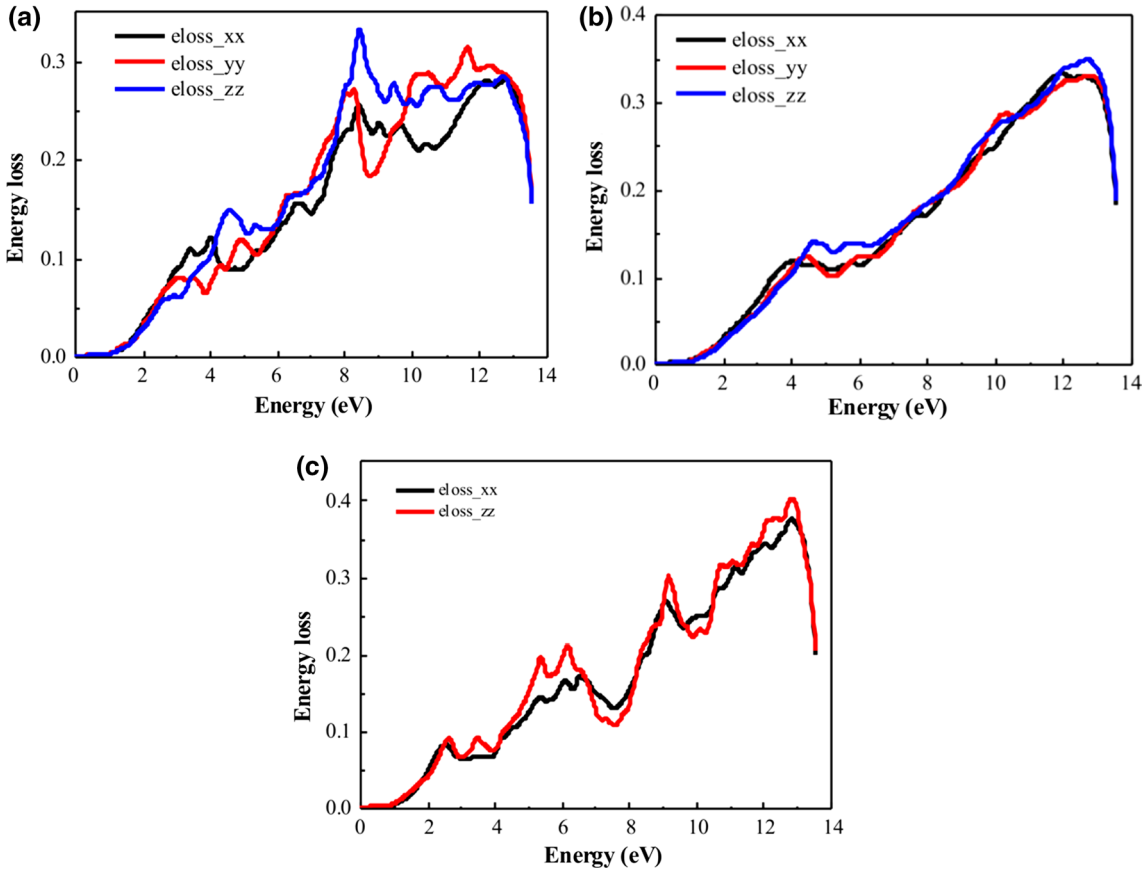

Fig. 8 Energy loss of Cu-Sb-S materials: (a) $CuSbS_2$, (b) Cu_3SbS_3 and (c) Cu_3SbS_4.

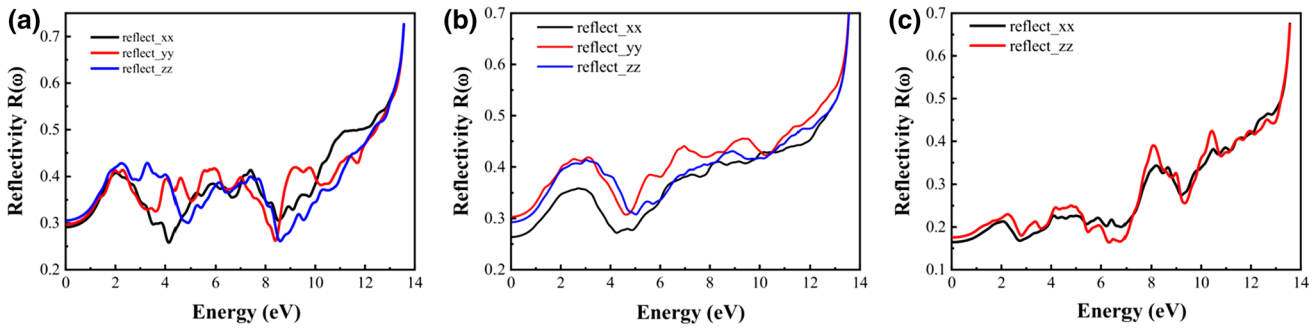

Fig. 9 Reflectivity of Cu-Sb-S materials: (a) $CuSbS_2$, (b) Cu_3SbS_3 and (c) Cu_3SbS_4.

shows that in this region the compounds no longer absorb light. The refractive index values n(ω) of $CuSbS_2$, Cu_3SbS_3 and Cu_3SbS_4 are depicted in Fig. 10a, b, and c, respectively. At zero frequency limit ($\omega = 0$), the average static refractive index $n(0)$ amounts to 3.40 for $CuSbS_2$, 3.31 for Cu_3SbS_3, and 2.32 for Cu_3SbS_4 indicating that the refractive index of $CuSbS_2$ and Cu_3SbS_3 are close to each other, whereas that of Cu_3SbS_4 is one unit smaller. At finite photon frequencies the refractive index exhibits a maximum at around 1.9 eV and then drops to reach about 3, 3.2 and 2.3 for $CuSbS_2$, Cu_3SbS_3 and Cu_3SbS_4, respectively, at $\hbar\omega$ ~ 2.3 eV, which corresponds to the mid spectrum energy of visible light. Hence, the speed of light in $CuSbS_2$ and Cu_3SbS_3 is substantially smaller than in Cu_3SbS_4 but more importantly, assuming normal incidence, light is almost twice more reflected by $CuSbS_2$ and Cu_3SbS_3 (29%) than by Cu_3SbS_4 (16%). The low reflectivity of Cu_3SbS_4 may counteract the small polarizability of its own bonds, which

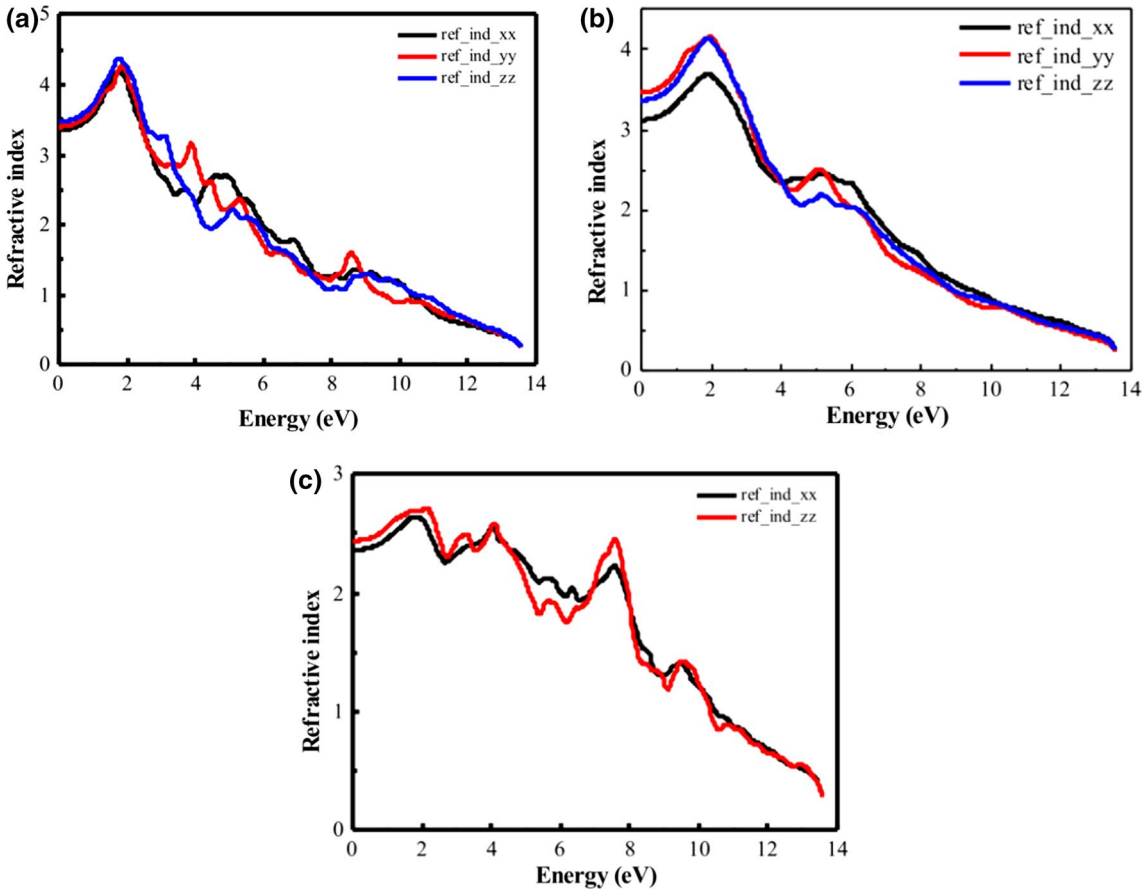

Fig. 10 Refractive index of Cu-Sb-S materials: (a) $CuSbS_2$, (b) Cu_3SbS_3 and (c) Cu_3SbS_4.

has been assumed to induce lower absorption coefficient (see above).

Conclusions

The electronic, QTAIM topological, and optical characteristics of $CuSbS_2$, Cu_3SbS_3, and Cu_3SbS_4 compounds have been theoretically explored by utilizing WIEN2k package to provide fundamental insights and understand their relevance applicability for photovoltaics. The $CuSbS_2$, Cu_3SbS_3, and Cu_3SbS_4 exhibit band gap energy of 1.18 eV, 1.28 eV, and 1.0 eV, respectively, which are mainly attributed to a strong Cu-3d and S-3p orbitals hybridization in VBM and Sb-5p/Sb-5s orbitals and S-3p orbital mixing in CBM. The three Cu-Sb-S compounds exhibit high absorption coefficient ($> 10^4$ cm^{-1}) with relative stability in visible light region. The electron density topological studies revealed that the Cu-S bonds in $CuSbS_2$, Cu_3SbS_3, and Cu_3SbS_4 have close bonding characteristics, though not strictly the same due to the difference in atoms environment. Indeed, the Cu-S and Sb-S bonds are located in the transit zone according to Espinosa's definition, the former bonds being more ionic in nature and the latter being more covalent, as evidenced from the bond degree and $|V|/G$ ratio at the bond critical points. Interestingly, the Cu-S and Sb-S bonds in Cu_3SbS_4 are more covalent than in the other compounds, as assumed from smaller electron density Laplacian. In addition, non-localized interactions prevail in Sb-Sb and Cu-Cu bonds in $CuSbS_2$ and Cu_3SbS_3, respectively, but no such interactions exist in Cu_3SbS_4. Overall, these characteristics make the bonding network more rigid, or less polarizable, in this compound, which could be correlated to the lower absorption coefficient of Cu_3SbS_4. This, in turn, could suggest that Cu_3SbS_4 is less suitable for optical applications than $CuSbS_2$ and Cu_3SbS_3. This study brings new results on electronic and optical properties of $CuSbS_2$, Cu_3SbS_3, and Cu_3SbS_4 as well as original ones on their bonding characteristics. In the electronic and optical properties investigations already published, although the authors used HSE06 functional, the band gap was either under- or overestimated in comparison with experimental data, which could negatively impact the optical properties. Our work evidences that the HSE06 functional yields good electronic gaps and properties, provided

that well converged technical parameters (plane wave cutoff energy and k-point grid) are employed. The setting of these parameters is a limiting factor for DFT investigations. In future work this study will be extended by combining macroscopic properties with microscopic ones into a quantitative structure-property relationship model that will allow for the design of efficient materials.

Supplementary Information The online version contains supplementary material available at https://doi.org/10.1007/s11664-022-09650-3.

Acknowledgments The authors acknowledge the Egyptian-French cooperation program provided by the French Institute and the Science and Technology Fund (STDF-IFE) in Egypt, Grant No. 31127 for the financial support. This work was granted access to the HPC resources of the Centre Informatique National de l'Enseignement Supérieur (CINES), Montpellier, France under allocation A0090806881 made by the Grand Equipement National de Calcul Intensif (GENCI). It was also granted access to the HPC resources of Aix-Marseille University financed by the project Equip@Meso (ANR-10-EQPX-29-01) of the program "Investissements d'Avenir" supervised by the Agence Nationale de la Recherche.

Conflict of interest The authors declare that they have no conflict of interest.

References

1. Y.-Y. Sun, M.L. Agiorgousis, P. Zhang, and S. Zhang, Chalcogenide Perovskites for Photovoltaics. *Nano Lett.* 15, 581 (2015).
2. B. Yang, L. Wang, J. Han, Y. Zhou, H. Song, S. Chen, J. Zhong, L. Lv, D. Niu, and J. Tang, $CuSbS_2$ as a Promising Earth-Abundant Photovoltaic Absorber Material: A Combined Theoretical and Experimental Study. *Chem. Mater.* 26, 3135 (2014).
3. K. Ramasamy, H. Sims, W.H. Butler, and A. Gupta, Selective Nanocrystal Synthesis and Calculated Electronic Structure of all Four Phases of Copper–Antimony–Sulfide. *Chem. Mater.* 26, 2891 (2014).
4. T.K. Todorov, J. Tang, S. Bag, O. Gunawan, T. Gokmen, Y. Zhu, and D.B. Mitzi, Beyond 11% Efficiency: Characteristics of State-of-the-Art $Cu_2ZnSn(S, Se)4$ Solar Cells. *Adv. Energy Mater.* 3, 34 (2013).
5. F. Mohamadkhani, M. Heidariramsheh, S. Javadpour, E. Ghavaminia, S.M. Mahdavi, and N. Taghavinia, Sb_2S_3 and Cu_3SbS_4 Nanocrystals as Inorganic Hole Transporting Materials in Perovskite Solar Cells. *Sol. Energy* 223, 106 (2021).
6. L. Lin, G. Chen, L. Yao, Z. Huang, H. Li, F. Wu, W. Lin, Y. Mao, and Z. Huang, Antimony Loss and Composition-Dependent Phase Evolution of $CuSbS_2$ Absorber Using Oxides Nanoparticles Ink. *Mater. Sci. Semicond. Process.* 133, 105944 (2021).
7. N. Chlibi, J.P.B. Silva, E.M.F. Vieira, L.M. Goncalves, J.A. Moreira, A. Chahboun, H. Dahman, M. Pereira, M.J.M. Gomes, and E.L. Mir, Touch Sensor and Photovoltaic Characteristics of $CuSbS_2$ Thin Films. *Ceramics Int.* 47, 22594 (2021).
8. S.A. Zaki, M.I. Abd-Elrahman, A.A. Abu-Sehly, N.M. Shaalan, and M.M. Hafiz, Solar Cell Fabrication from Semiconducting Cu_3SbS_3 on n-Si: Parameters Evolution. *Mater. Sci. Semicond. Process.* 115, 105123 (2020).
9. G.K. Gupta and A. Dixit, Simulation Studies on Photovoltaic Response of Ultrathin $CuSb(S/Se)_2$ Ternary Compound Semiconductors Absorber-Based Single Junction Solar Cells. *Int. J. Energy Res.* 44, 3724 (2020).
10. B.H. Kumar, S. Shaji, and M.C.S. Kumar, Effect of Substrate Temperature on Properties of Co-evaporated Copper Antimony Sulfide Thin Films. *Thin Solid Films* 697, 137838 (2020).
11. L. Wan, X. Guo, Y. Fang, X. Mao, H. Guo, J. Xu, and R. Zhou, Spray Pyrolysis Deposited $CuSbS_2$ Absorber Layers For Thin-Film Solar Cells. *J. Mater. Sci.* 30, 21485–21494 (2019).
12. S. Banu, Y. Cho, K. Kim, S.K. Ahn, J. Gwak, and A. Cho, Phase Transition Behavior and Defect Analysis of $CuSbS_2$ Thin Films for Photovoltaic Application Prepared by Hybrid Inks. *Sol. Energy* 188, 1209–1220 (2019).
13. G. Han, J.W. Lee, and J. Kim, Fabrication and Characterization of Cu_3SbS_4 Solar Cell with Cd-Free Buffer. *J. Korean Phys. Soc.* 73, 1794 (2018).
14. L. Yu, R.S. Kokenyesi, D.A. Keszler, and A. Zunger, Inverse Design of High Absorption Thin-Film Photovoltaic Materials. *Adv. Energy Mater.* 3, 43 (2013).
15. R.F.W. Bader, *Atoms in Molecules* (Oxford: Clarendon Press, 1990).
16. A. Gassoumi, H.-E.M. Musa Saad, S. Alfaify, T.B. Nasr, and N. Bouariss, The Investigation of Crystal Structure, Elastic and Optoelectronic Properties of $CuSbS_2$ and $CuBiS_2$ Compounds for Photovoltaic Applications. *J. Alloys Compd.* 725, 181 (2017).
17. M. Kumar and C. Persson, $CuSbS_2$ and $CuBiS_2$ as Potential Absorber Materials for Thin-Film Solar Cells. *J. Renew. Sustain. Energy* 5, 031616 (2013).
18. T. Maeda and T. Wada, First-Principles Study of Electronic Structure of $CuSbS_2$ and $CuSbSe_2$ Photovoltaic Semiconductors. *Thin solid film* 582, 401 (2015).
19. J. Li, X. Han, J. Li, Y. Zhao, and C. Fan, Structural, Electronic and Optical Properties of Famatinite and Enargite Cu_3SbS_4 Under Pressure: A Theoretical Investigation. *Phys. Status Solidi (b)* 254, 1600608 (2017).
20. P. Blaha, K. Schwarz, G.K.H. Madsen, D. Kvasnicka, and J. Luitz, *WIEN2k, an Augmented Plane Wave + Local Orbitals Program for Calculating Crystal Properties Karlheinz Schwarz* (Austria: Techn. Universität Wien, 2001).
21. J.P. Perdew, K. Burke, and M. Ernzerhof, Generalized Gradient Approximation Made Simple. *Phys. Rev. Lett.* 77, 3865 (1996).
22. D. Koller, F. Tran, and P. Blaha, Merits and Limits of the Modified Becke–Johnson Exchange Potential. *Phys. Rev. B* 83, 195134 (2011).
23. W. Khan and A.H. Reshak, Optoelectronic and Thermoelectric Properties of $KAuX_5$ (X = S, Se): A First Principles Study. *J. Mater. Sci.* 49, 1179 (2014).
24. F. Tran and P. Blaha, Accurate Band Gaps of Semiconductors and Insulators with a Semilocal Exchange-Correlation Potential. *Phys. Rev. Lett.* 102, 226401 (2009).
25. J. Heyd, G.E. Scuseria, and M. Ernzerhof, Hybrid Functionals Based on a Screened Coulomb Potential. *J. Chem. Phys.* 118, 8207 (2003).
26. C. Ambrosch-Draxl and J. Sofo, Linear Optical Properties of Solids Within the Full-Potential Linearized Augmented Planewave Method. *Comput. Phys. Commun.* 175, 1 (2006).
27. A. Otero-de-la-Roza, E.R. Johnson, and V. Luaña, Critic2: A Program for Real-Space Analysis of Quantum Chemical Interactions in Solids. *Comput. Phys. Commun.* 185, 1007 (2014).
28. J.T.R. Dufton, A. Walsh, P.M. Panchmatia, L.M. Peter, D. Colombara, and M.S. Islam, Structural and Electronic Properties of $CuSbS_2$ and $CuBiS_2$: Potential Absorber Materials for Thin-Film Solar Cells. *Phys. Chem. Chem. Phys.* 14, 7229 (2012).
29. D. Xu, S. Shen, Y. Zhang, H. Gu, and Q. Wang, Selective Synthesis of Ternary Copper-Antimony Sulfide Nanocrystals. *Inorg. Chem.* 52, 12958 (2013).
30. K. Nefzi, A. Rabhi, and M. Kanzari, Investigation of Physical Properties and Impedance Spectroscopy Study of Cu_3SbS_3 Thin Films. *J. Mater. Sci. Mater. Electron.* 27, 1888 (2016).

31. J. Embden and Y. Tachibana, Synthesis and Characterisation of Famatinite Copper Antimony Sulfide Nanocrystals. *J. Mater. Chem.* 22, 11466 (2012).
32. K. Chen, C. Di Paola, B. Du, R. Zhang, S. Laricchia, N. Bonini, C. Weber, I. Abrahams, H. Yan, and M. Reece, Enhanced Thermoelectric Performance of Sn-Doped Cu_3SbS_4. *J. Mater. Chem. C* 6, 8546 (2018).
33. P. Jiang, P. Boulet, and M.-C. Record, A DFT Study of the Electronic, Optical and Topological Properties of Free and Biaxially Strained $CuIn_{1-x}Al_xSe_2$. *J. Mater. Chem. C* 7, 5803 (2019).
34. S. Ikeda, S. Sogawa, Y. Tokai, W. Septina, T. Harada, and M. Matsumura, Selective Production of $CuSbS_2$, Cu_3SbS_3, and Cu_3SbS_4 Nanoparticles Using a Hot Injection Protocol. *RSC Adv.* 4, 40969 (2014).
35. M.E. Edley, B. Opasanont, J. Conley, H. Tran, S.Y. Smolin, S. Li, A.D. Dillon, A.T. Fafarman, and J.B. Baxter, Solution Processed $CuSbS_2$ Films For Solar Cell Applications. *Thin Solid Films* 646, 180 (2018).
36. A. Hussain, R. Ahmed, N. Ali, A. Shaari, J.-T. Luo, and Y.Q. Fu, Characterization of Cu_3SbS_3 Thin Films Grown by Thermally Diffusing Cu_2S and Sb_2S_3 Layers. *Surf. Coat. Technol.* 319, 294 (2017).
37. X. Qiu, S. Ji, C. Chen, G. Liu, and C. Ye, Synthesis, Characterization, and Surface-Enhanced Raman Scattering of Near Infrared Absorbing Cu_3SbS_3 Nanocrystals. *Cryst. Eng. Commun.* 15, 10431–10434 (2013).
38. G.H. Albuquerque, K. Kim, J. Lopez, A. Devaraj, S. Manandhar, Y. Liu, J. Guo, C. Chang, and G. Herman, Multimodal Characterization of Solution-Processed Cu_3SbS_4 Absorbers for Thin Film Solar Cells. *J. Mater. Chem. A* 6, 8682 (2018).
39. U. Chalapathi, B. Poornaprakash, and S.-H. Park, Growth and Properties of Cu_3SbS_4 Thin Films Prepared by a Two-Stage Process for Solar Cell Applications. *Ceram. Int.* 43, 5229 (2017).
40. O. Madelung, *Semiconductors: Data Handbook* (New York: Springer, 2000).
41. J. Embden, K. Latham, N.W. Duffy, and Y. Tachibana, Near-Infrared Absorbing $Cu_{12}Sb_4S_{13}$ and Cu_3SbS_4 Nanocrystals: Synthesis, Characterization, and Photoelectrochemistry. *J. Am. Chem. Soc.* 135, 11562 (2013).
42. Q. Zeng, Y. Di, C. Huang, K. Sun, Y. Zhao, H. Xie, D. Niu, L. Jiang, X. Hao, Y. Lai, and F. Liu, Famatinite Cu_3SbS_4 Nanocrystals as Hole Transporting Material for Efficient Perovskite Solar Cells. *J. Mater. Chem. C* 6, 7989 (2018).
43. A. Walsh and G.W. Watson, The Origin of the Stereochemically Active Pb(II) Lone Pair: DFT Calculations on PbO and PbS. *J. Solid State Chem.* 178, 1422 (2005).
44. H. Yang, P. Boulet, and M.-C. Record, A Rapid Method for Analyzing the Chemical Bond From Energy Densities Calculations at the Bond Critical Point. *Comput. Theor. Chem.* 1178, 112784 (2020).
45. E. Espinosa, I. Alkorta, J. Elguero, and E. Molins, From Weak to Strong Interactions: A Comprehensive Analysis of the Topological and Energetic Properties of the Electron Density Distribution Involving X-H….F–Y Systems. *J. Chem. Phys.* 117, 5529 (2002).
46. B. Amin, R. Khenata, A. Bouhemadou, I. Ahmad, and M. Maqbool, Opto-Electronic Response of Spinels $MgAl_2O_4$ and $MgGa_2O_4$ Through Modified Becke–Johnson Exchange Potential. *Physica B* 407, 2588 (2002).
47. D.R. Penn, Wave-Number-Dependent Dielectric Function of Semiconductors. *Phys. Rev.* 128, 2093 (1962).
48. M. Fox, in *Optical Properties of Solids* (Oxford U.P., New York, 2001).
49. J. Palisaitis, C.-L. Hsiao, M. Junaid, J. Birch, L. Hultman, and P.O.A. Persson, Effect of Strain on Low-Loss Electron Energy Loss Spectra of Group-III Nitrides. *Phys. Rev. B* 84, 245301 (2011).